

# H<sub>2</sub>-Dependent Carbon Dissolution and Diffusion-Out in Graphene Chemical Vapor Deposition Growth

Baoshan Hu,<sup>\*,†,‡</sup> Yan Jin,<sup>†</sup> Dongjie Guan,<sup>§</sup> Zhengtang Luo,<sup>||</sup> Bo Shang,<sup>\*,†</sup> Qianrui Fang,<sup>⊥</sup> and Haibo Ruan<sup>#</sup>

<sup>†</sup>School of Chemistry and Chemical Engineering and <sup>‡</sup>Chongqing Key Laboratory of Chemical Process for Clean Energy and Resource Utilization, Chongqing University, Chongqing, 400044, China

<sup>§</sup>College of Architecture and Urban Planning, Chongqing Jiaotong University, Chongqing, 400074, China

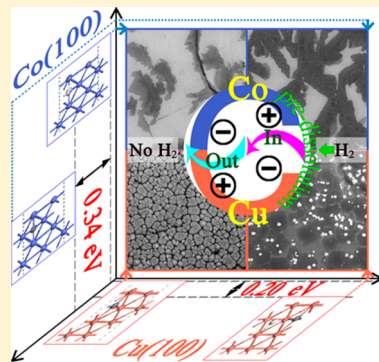
<sup>||</sup>Department of Chemical and Biomolecular Engineering, The Hongkong University of Science and Technology, Kowloon, Hong Kong

<sup>⊥</sup>Zhejiang Shengyuan Chemical Fiber Co. Ltd., Hangzhou, 311200, Zhejiang Province, China

<sup>#</sup>Research Institute for New Materials Technology, Chongqing University of Arts and Sciences, Yongchuan, Chongqing, 402160, China

## Supporting Information

**ABSTRACT:** Highlighting the roles of H<sub>2</sub> on the carbon dissolution and diffusion-out unit steps in the metal substrate is highly imperative to constitute a whole puzzle elucidating how the H<sub>2</sub> affects the graphene chemical vapor deposition (CVD) growth, taking into account that the effects of H<sub>2</sub> on the surface process have been intensively emphasized. In this article, we designed a series of graphene growth experiments by introducing the H<sub>2</sub> in the individual unit step on the Cu and Co films as a comparison due to their distinctively intrinsic carbon solubility. We investigated the effects of H<sub>2</sub> on the crystallographic structure, surface morphology, and chemical environment of metal substrates, and the thickness and quality of as-grown graphene films. We also established the theoretical models to monitor the interaction between carbon and metal atoms with and without H<sub>2</sub>. Our results demonstrate that the H<sub>2</sub> predissolution could suppress the carbon dissolution in the Cu film and enhance the diffusion-out of dissolved carbon atoms, whereas in the Co film the converse would occur.



## INTRODUCTION

Graphene, the atomic thin carbon film with honeycomb lattice, grows up a star material, due to its unique band structure and excellent electronic, optical, mechanical, and thermal properties. The recently developed chemical vapor deposition (CVD) method, using catalytic substrates, has emerged as a convenient technique to obtain high-quality and large-size graphene. A typical CVD process consists of four main elementary steps: (i) adsorption and catalytic decomposition of precursor gas, (ii) diffusion and dissolution of decomposed carbon species into bulk metal, (iii) segregation of dissolved carbon atoms onto the metal surface, and, finally, (iv) surface nucleation and growth of graphene.<sup>1</sup> The comprehensive understanding and effective controlling of the growth process has attracted intense effort for the precise regulation of domain structure, layer thickness, and stacking order aiming at practical applications.

In general, the graphene CVD growth process using metals with a certain carbon solubility, such as Ni and Co, involve all four elementary steps, whereas the carbon dissolution and segregation steps are negligible in the CVD process using metals with negligible carbon solubility, such as Cu. The CVD growth process typically uses a hydrocarbon gas feedstock mixed with H<sub>2</sub> flowing as a buffer component. In this process,

the carbon atoms coexist with hydrogen atoms on the surface of metal catalysts, and consequently their mutual interaction may change the adsorption and diffusion properties of carbon atoms and determine the graphene growth mechanism and kinetics. Thereby, the roles of H<sub>2</sub> over Cu metal catalyst have been intensively investigated experimentally. The H<sub>2</sub> can clean the Cu surface and reduce the surface oxide, as well as act as an activator and an etchant.<sup>2–5</sup> Especially the etching role of H<sub>2</sub> can be utilized in the controllable preparation in the thickness, shape, size, edge configuration, and crystallinity quality of graphene islands/domains.<sup>6–8</sup> Besides, some novel roles of H<sub>2</sub> have been revealed. For instance, Luo et al. suggested that H<sub>2</sub> could etch the Cu surface to produce small size nanoparticles that affected the graphene nucleation;<sup>9</sup> Tour et al. reported that the H<sub>2</sub>-associated edge nucleation growth mechanism permitted the fabrication of three-dimensional (3D) hexagonal graphene onion ring structures.<sup>10</sup> We confirmed that the H<sub>2</sub> introduced in the annealing process could be released to facilitate the high-quality graphene growth with no H<sub>2</sub> gas

Received: July 22, 2015

Revised: August 27, 2015

Published: September 30, 2015

supply in the growth time.<sup>11</sup> However, the low carbon solubility of Cu metal inevitably conceals deep insight into the effects of H<sub>2</sub> on the CVD process. As typical experimental evidence, the real-time investigations made on both the Cu and Ni substrates demonstrated that the competitive dissociative chemisorption of H<sub>2</sub> and dehydrogenating chemisorption of methane (CH<sub>4</sub>), and the competition of diffusion between H<sub>2</sub> and carbon species dominated the growth kinetics of CVD-grown graphene very distinctively.<sup>12</sup>

Several theoretical simulations were developed to investigate the different H<sub>2</sub> roles for graphene CVD growth over Cu and Ni metals. By using ab initio calculations, Zhang et al. revealed that the H<sub>2</sub> at high partial pressure could passivate the active graphene edge and allow the active carbon monomers to diffuse onto the graphene-covered Cu(111) surface to form the adlayer graphene, whereas the hydrogenation of graphene edge on Ni(111) surface did not play a dominant role due to the more stable Ni-passivated edge than the Cu-passivated edge.<sup>13</sup> Tour et al. claimed that this hydrogenation would decrease the energy of a carbon adatom near the growing edge by ~0.7 eV, which corresponded to an increase of adsorption probability by a factor of  $e^{\Delta E/kT} \sim 10^2$ , facilitating the nucleation of a new graphene layer near the growing edge of the previous layer.<sup>10</sup> Wang and Wu et al. studied the effects of H<sub>2</sub> on the CH<sub>4</sub> dissociation over Cu(111) and Ni(111) surfaces by density functional theory. They found that the adsorbed H atom accelerated the migration of C atoms and hindered the polymerization of the C atoms on Cu(111) which resulted in sufficient time for C atoms to be relaxed to the most stable site for a perfect graphene pattern formation, whereas the H atoms depressed the migration process and enhanced the polymerization for Ni(111), leading to little effect on the graphene nucleation rate.<sup>14</sup> In general, the roles of H<sub>2</sub> with either experimental or computational ways have mostly focused on the Cu-based surface processes involving the above i and iv elementary steps. It is additionally essential to investigate the effects of H<sub>2</sub> on the diffusion and dissolution of carbon atoms, and the further graphene growth by in parallel comparing metals with different carbon solubilities. Especially the roles of H<sub>2</sub> over catalyst metals with relatively large carbon solubility, such as Ni or Co, have been less demonstrated.

Herein, we deliberately designed a series of graphene growth experiments on the Cu and Co films by introducing the H<sub>2</sub> in the individual unit step to emphatically elucidate the effects of H<sub>2</sub> on the C diffusion/dissolution. Motivated by the experimental clues, we used the computational method based on the Vienna Ab initio Simulation Package (VASP) to interpret the effects of H<sub>2</sub> predissolution on the diffusion/dissolution behaviors of C atoms, as well as its effect on the interaction between C atoms and metals. The experimental and computational results illustrate that the H<sub>2</sub> predissolution suppresses the dissolution but enhances the diffusion-out of carbon atoms dissolved in the Cu bulk; conversely, the dissolution of carbon atoms into the Co bulk could be enhanced through electron transfer and covalent interaction. Our results are beneficial to understanding the roles of H<sub>2</sub> for advancing graphene processing and achieving better control of graphene structure.

## EXPERIMENTAL SECTION

**Experimental Methods.** Cu and Co films were deposited onto clean SiO<sub>2</sub> (300 nm)/Si substrates by a magnetron ion sputtering machine (Shenyang Scientific Instrument Develop-

ment Center of CAS, JGP450) with an argon atmosphere of 0.6 Pa and a sputtering power of 150 W for 60 min. Then, the Cu or Co film was placed on a quartz tray and inserted into the center of a quartz tube furnace. The Cu or Co film was heated to the growth temperature of 1000 °C at a heating ramp rate of 12 °C/min and then annealed for 30 min in a gas flow of Ar or Ar/H<sub>2</sub>, followed by the introduction of CH<sub>4</sub> for 3 min of graphene growth. Finally, the quartz tray was pulled out of the furnace for rapid cooling. The transfer process is the same as in our previous work.<sup>11</sup> The poly(methyl methacrylate) (PMMA) layer was spin-coated onto the graphene-covered metal film and heated at 90 °C for 10 min. The Cu or Co film was dissolved in FeCl<sub>3</sub>/HCl aqueous solution. The PMMA/graphene was washed with deionized water and transferred onto a target SiO<sub>2</sub>/Si substrate and heated at 120 °C for 30 min. Finally, the PMMA was removed with acetone.

An optical micrograph of transferred graphene was measured with a BX-51 microscope (Olympus, Japan). Raman spectroscopy of graphene was measured with a LabRAM HR Evolution (HORIBA Scientific, Japan) using a green laser of 532 nm excitation wavelength. Scanning electron microscopy (SEM) images were obtained using a JSM-7800F (JEOL, Japan). Atomic force microscopy (AFM) measurements were performed with an MFP-3D (OXFORD Instruments Asylum Research, U.K.). Electron backscatter diffraction (EBSD) patterns were obtained using a Zeiss AURIGA FIB/SEM (Carle Zeiss, Germany). X-ray diffraction (XRD) measurements of Cu and Co films were carried out using a SHIMADZU XRD-6000 (Shimadzu, Japan). X-ray photoelectron spectroscopy (XPS) of the as-grown graphene samples on the metal films was analyzed with an Escalab 250 (Thermo Scientific, USA).

**Computational Methods.** All the calculations were performed with the Vienna Ab initio Simulation Package (VASP). The PAW-PBE methods have been employed to describe the interaction between the electrons and the ions. A plane-wave basis set with a kinetic energy cutoff of 450 eV was used. The Monkhorst–Pack scheme K-point grid sampling was set as 5 × 5 × 1. In the structural optimization process, the energy change, maximum force, maximum stress, and maximum displacement were set as  $1.0 \times 10^{-6}$  eV/atom, 0.05 eV/Å, 0.1 GPa, and 0.001 Å, respectively.

In our calculations, the Cu(100) and ferromagnetic nonpolar fcc Co(100) surfaces have been mainly considered based on the XRD results. The calculations based on the 100 facet were appealing, because a large amount of literature has picked up the 111 facet to construct the models and because of the fact that the Cu foil used conventionally for the graphene CVD growth was preferred along the [100] direction.<sup>11</sup> For all the calculations, the five layers of 2 × 2 periodic metal slab models were adopted and the Brillouin zones were sampled by 5 × 5 × 1 grid meshes based on the Monkhorst–Pack scheme. For both types of metal (M) surfaces, the formation energies were defined as  $E_f = E[C@H@M(100)] - E[M(100)] - E(C) - E(H)$  with the H<sub>2</sub> predissolution and  $E_f = E[C@M(100)] - E[M(100)] - E(C)$  without the H<sub>2</sub>, where the E terms represent the energies of different slabs, free energies of carbon and hydrogen atoms based on graphene and hydrogen molecules. To understand the difference between the interactions of the carbon atoms and metals, the properties of the enthalpy, transition states (TS), and crystal orbital Hamilton population (COHP) have been considered. The C-NEB methods were employed to get the transition states (TS)

of carbon migration in the metal bulk. The lobster and wxDragon programs were used to investigate the COHP results.

## RESULTS AND DISCUSSION

Displayed in Figure 1 are the electron backscatter diffraction (EBSD) patterns of graphene/Cu films and graphene/Co films

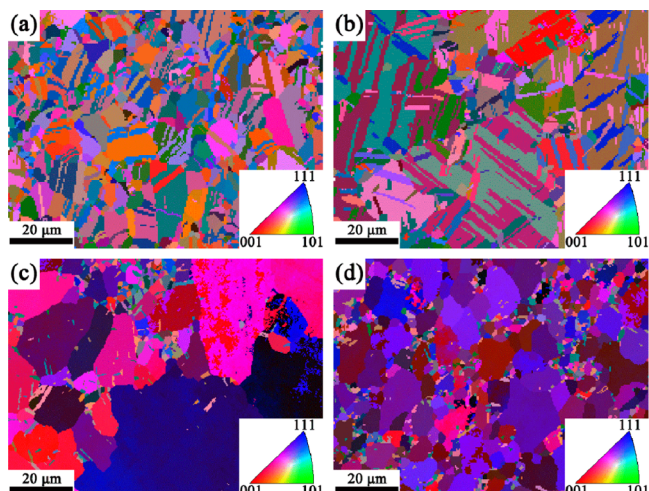


**Figure 1.** Electron backscatter diffraction (EBSD) patterns of metal films after graphene CVD growth with and without H<sub>2</sub> during the synthesis process. Cu films: (a) with H<sub>2</sub> and (b) without H<sub>2</sub>, Co films: (c) with H<sub>2</sub> and (d) without H<sub>2</sub>.

grown with and without H<sub>2</sub> in the whole synthesis process. It is evidenced that all the Cu and Co metal surfaces were composed of various crystal planes marked with different colors in the EBSD patterns, indicating the polycrystalline nature of metal films. The Cu films with and without H<sub>2</sub> had almost the same distributions of crystal planes, and the statistical histograms of grain size for Cu and Co films listed in Figure S-1 show that the participation of H<sub>2</sub> did not alter the

grain size apparently. This is a different case from the Cu foil which had relatively larger grain sizes in the presence of H<sub>2</sub> than without H<sub>2</sub>.<sup>11</sup> The different effects of H<sub>2</sub> may originate from distinctive surface structure and growth kinetics between Cu film and Cu foil, as demonstrated in our previous work.<sup>15</sup> The Co film with the participation of H<sub>2</sub> in the graphene synthesis process had a few grains of very large size around 30 μm (see Figure 1c and Figure S-1c) as compared to the Co film without H<sub>2</sub>. Note that the diffusion coefficient of H<sub>2</sub> in Cu is relatively as high as  $2 \times 10^{-4} \text{ cm}^2 \text{ s}^{-1}$ .<sup>12</sup> It is thus plausible that a considerable amount of H<sub>2</sub> dissolution into the Cu metal was not the dominant influencing factor to the metal crystallographic structure in the graphene CVD growth, whereas it is likely that H<sub>2</sub> would play essential roles in the metal surface morphology and successive graphene growth on the metal films.

SEM and corresponding AFM images of Cu and Co metal surfaces after graphene growth with and without H<sub>2</sub> are displayed in Figure 2. For the Cu films, one can see from the SEM image in Figure 2a that the presence of H<sub>2</sub> resulted in the smooth surface and obvious graphene flakes with clear boundaries to the Cu surface covering the metal surface. The white particles on the surfaces in Figure 2a,b,e,f were ascribed to the sublimation of Cu films as reported recently.<sup>15,16</sup> For the Co films, the surface was much smoother with H<sub>2</sub> than without H<sub>2</sub> as seen from the AFM images (Figure 2g,h). No Co particles were observed due to a higher melting point of Co metal than Cu metal. Meanwhile, more graphene flakes were grown on the Co film with H<sub>2</sub> as shown in the SEM images (Figure 2c,d).

We then used X-ray photoelectron spectroscopy (XPS) to investigate the bonding types between C atoms and/or other possible atoms considering the different chemical reaction environments with and without H<sub>2</sub> participation, as listed in Figure 3. In general, the deconvolution of C 1s XPS spectra shows four distinctive peaks associated with C–C sp<sup>2</sup> at ~284.6 eV, C–C sp<sup>3</sup> at ~285.2 eV, C–OH at ~286.4 eV, and O=C—OH at ~288.3 eV.<sup>17</sup> Using Cu films, the presence of H<sub>2</sub>

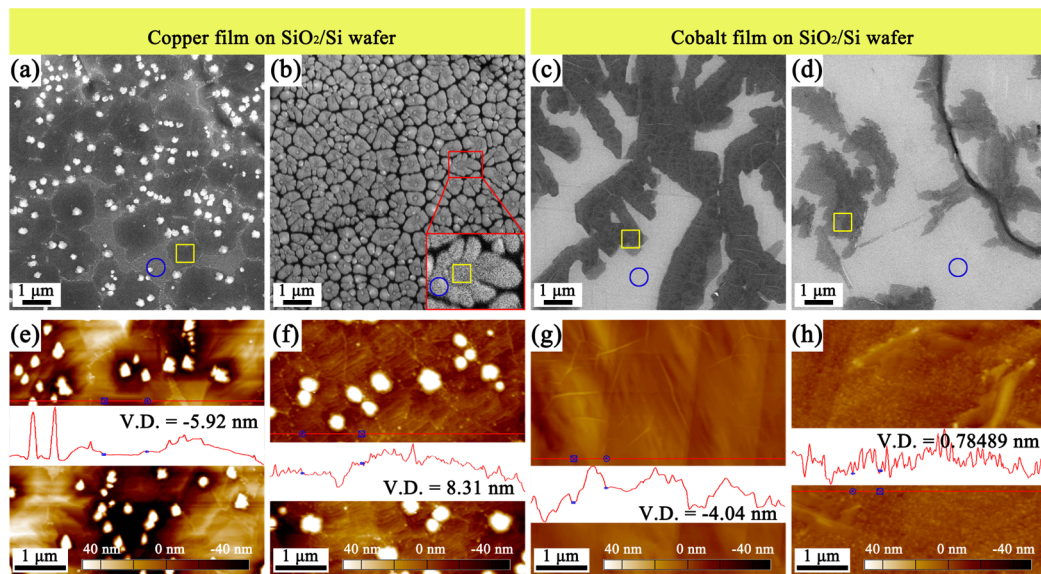


**Figure 2.** SEM (a–d) and corresponding AFM (e, f) images of metal films after graphene CVD growth with and without H<sub>2</sub> during the synthesis process. Cu films: (a) and (e) with H<sub>2</sub>, (b) and (f) without H<sub>2</sub>. Co films: (c) and (g) with H<sub>2</sub>, (d) and (h) without H<sub>2</sub>. In the SEM images, the yellow squares indicate the graphene regions, while the blue circles indicate the metal regions.

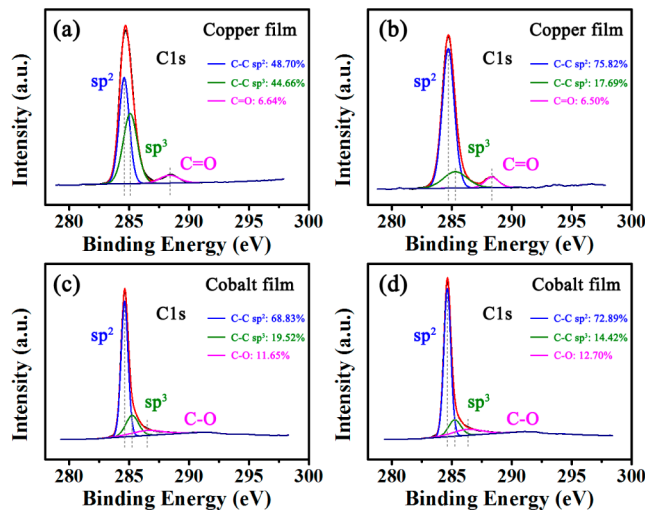


**Figure 3.** XPS C 1s spectra of as-received graphene films on metal films after reactions. (a) Graphene/Cu film grown with H<sub>2</sub>; (b) graphene/Cu film grown without H<sub>2</sub>; (c) graphene/Co film grown with H<sub>2</sub>; (d) graphene/Co film grown without H<sub>2</sub>.

increased the percentage of sp<sup>3</sup> carbon bond dramatically; differently, the H<sub>2</sub> did not alter the ratio of sp<sup>2</sup> and sp<sup>3</sup> carbon bonds when using Co films. This is an indication that the H<sub>2</sub> could greatly affect the segregation of carbon atoms on the Cu surface and cocatalyze the formation of sp<sup>3</sup> carbon bonds in the graphene framework, whereas the H<sub>2</sub> did not exert significant roles in the formation of carbon bonds on the Co surface due to the first dissolution-in and successive segregation of carbon atoms.

Unlike previous reports that the adsorbed oxygen atoms prefer to form epoxide groups on the graphene basal plane due to their lowest energy configuration,<sup>18–20</sup> here, the O-containing groups were bonded with the C atoms by a single covalent bond of C—OH at a peak of 286.4 eV on the Cu metal, but by a double covalent bond of O=C—OH at a peak of 288.3 eV on the Co metal. Emphatically, the atomic

percentages of O-containing groups were not affected by whether the H<sub>2</sub> was present or not, but only by the catalyst metals. Additionally, we can exclude the potential linkage between sp<sup>2</sup>/sp<sup>3</sup> carbon bond ratios and the bond types of C—O/C=O. Such a considerable influence of substrate on the O-containing group adsorption was also revealed on the Ir and Pt metals.<sup>21</sup> These hydroxyl radicals of graphene grown on the Cu metal may be generated from moisture in the ambient air or physisorbed water molecules. As far as the formation of C—O and C=O bonds is concerned, it is reasonable that the migration of a hydrogen atom induced by a weak hydrogen bond between two adjacent hydroxyl groups may form a carbonyl group due to a stronger interaction between graphene and Co metal;<sup>22</sup> then, these carbonyl groups can be transformed to carboxyl groups by a rapid reaction between them and hydroxyl radicals.<sup>22</sup> The carboxyl groups are relatively stable, and further reaction with atomic oxygen or hydroxyl radical is very unlikely.<sup>23</sup> Our finding provides valuable guidance for the controllable modification and functionalization of the graphene toward extensive applications. Thus, these results suggest that the roles of H<sub>2</sub> in the formation of chemical bonds between carbon atoms, as well as the chemical reactivity of carbon atoms, are intensively dependent on the catalyst metals.

To further discriminate the effects of H<sub>2</sub> on the individual carbon dissolution and diffusion-out steps, we designed a series of growth experiments with introducing H<sub>2</sub> in various stages of heating, annealing, growth (introducing CH<sub>4</sub>), and cooling, e.g., (i) in all steps, (ii) in all steps except for the growth, (iii) not introducing H<sub>2</sub> in all steps with the two selected CH<sub>4</sub> flow rates of 3 and 10 sccm, and (iv) only introducing H<sub>2</sub> in the growth, as noted in Figure 4. We first exclude the possibility of metal crystallography transformation under so distinctive growth conditions by the EBSD patterns in Figure 1 and the XRD characterizations in Figure S-2. Strikingly, graphene could be successfully grown even without H<sub>2</sub> in the whole process on both the Cu and Co films. This is quite different from the graphene growth on the Cu foil in our previous data where the graphene could not be synthesized in the absence of H<sub>2</sub> flow.<sup>11</sup>

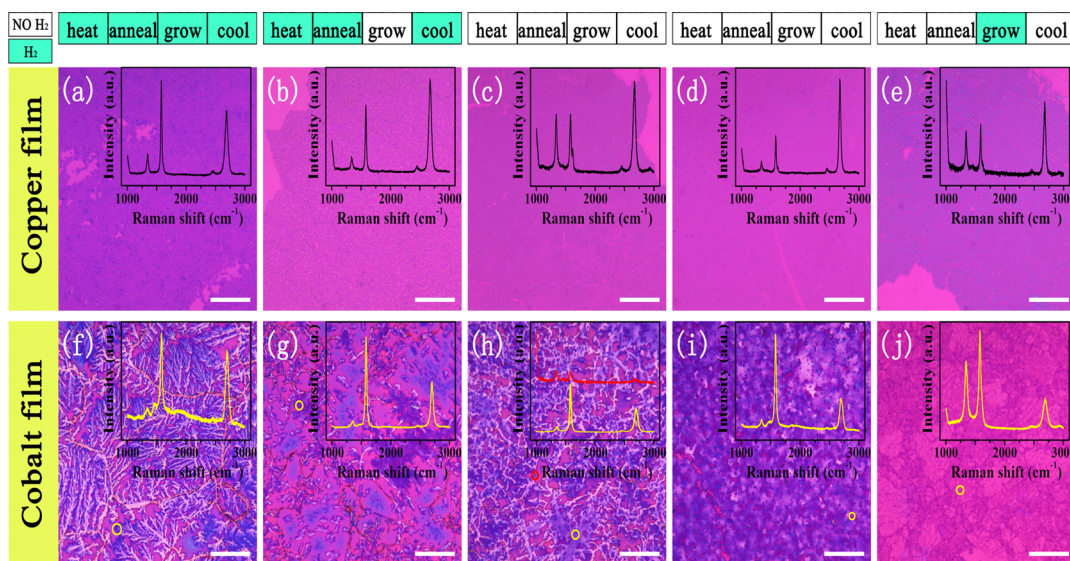


**Figure 4.** Optical micrographs (OM) and representative Raman spectra of graphene films transferred onto SiO<sub>2</sub>/Si substrate (a–e, f–j). Panel (a) indicates the H<sub>2</sub> participating in the entire process; (b) only in growth step without H<sub>2</sub>; (c) without H<sub>2</sub> in entire process; (d) without H<sub>2</sub> but changing the CH<sub>4</sub> flow rate from the standard 3 sccm to 10 sccm; (e) with H<sub>2</sub> only in growth step.

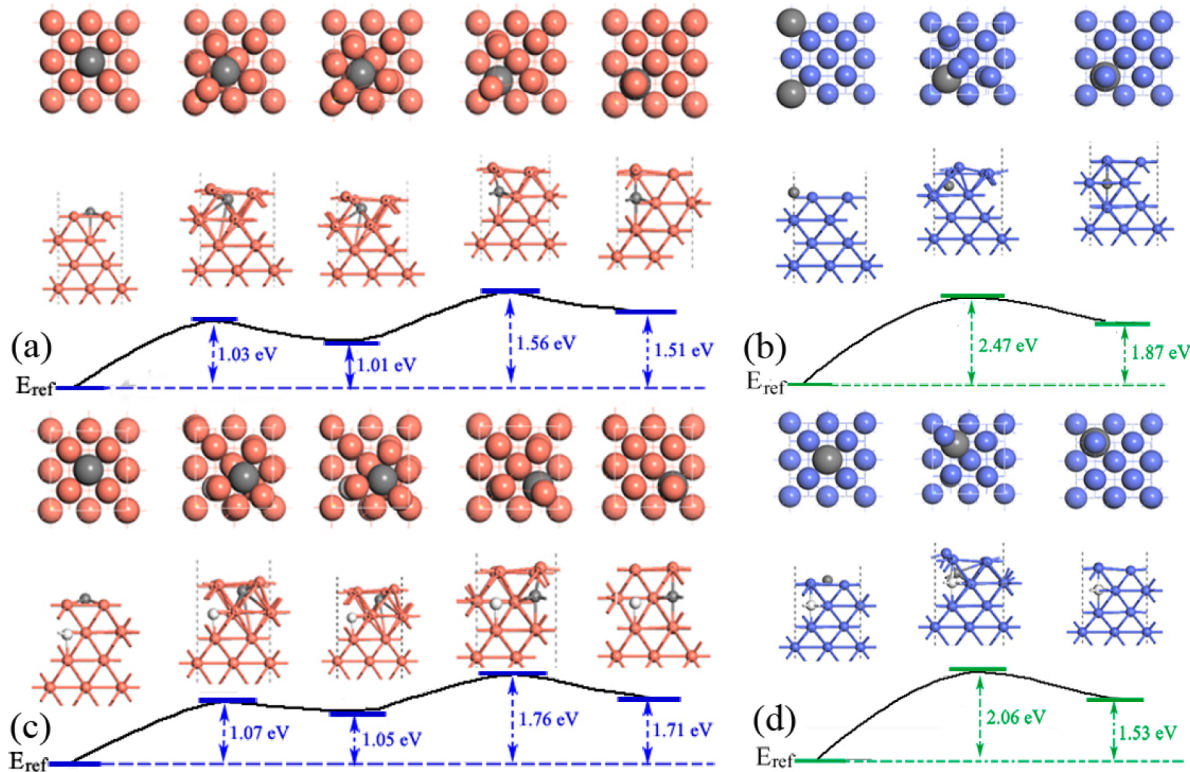


**Figure 5.** Top views, side views, and energy profiles of the C monomer diffusing from the Cu(100) (left panel) and Co(100) (right panel) surfaces to metal subsurfaces. (a, b) Before and (c, d) after H<sub>2</sub> predissolution. The gray spheres in (a)–(d) indicate the C atoms, and the white spheres in (c) and (d) indicate the H atoms. The benchmark energies  $E_{\text{ref}}$  are based on the models with the lowest energy.

The H<sub>2</sub>-free process is advanced due to the safety issue. Until now, only Kong et al. succeeded in the H<sub>2</sub>-excluded graphene synthesis via atmospheric pressure CVD,<sup>24</sup> besides, plasma-enhanced and rapid thermal CVD processes have been reported for the H<sub>2</sub>-free graphene fabrication.<sup>25,26</sup>

For the Cu film, it was seen that the as-grown graphene films in all cases were single or few layers due to the low carbon solubility of the Cu metal. The comparison analysis of OM and Raman spectra in Figure 4c,e showed that the graphene films grown with and without H<sub>2</sub> in the growth stage had similar thickness and crystalline quality. The data specified that H<sub>2</sub> did not act as a cocatalyst for enhancing the CH<sub>4</sub> decomposition as claimed previously,<sup>5</sup> when no H<sub>2</sub> was introduced in the heating and annealing steps. Moreover, several H<sub>2</sub>-associated surface processes,<sup>10,27</sup> which have been reported to contribute to the growth of thick graphene films, did not play essential roles in affecting the graphene thickness in our system. However, it is also compared in Figure 4a,e that the presence of H<sub>2</sub> in the heating and anneal steps resulted in the relatively thick graphene film, as indicated by some deep color spots in the optical micrograph and higher Raman G/2D intensity ratio in the inset of Figure 4a. Such a difference could not be explained by the much rougher Cu surface without H<sub>2</sub> than that with H<sub>2</sub> as seen the SEM images in Figure 2a,b. Therefore, we speculate that the predissolution of H<sub>2</sub> in the Cu metal during the heating and annealing steps (Figure 4a,b), because of large H solubility in the Cu metal,<sup>12</sup> should increase the dissolution abundance in the growth step and/or diffusion-out of carbon atoms in the cooling step, thus leading to the slight increase of thickness. Based on these distinctive roles of H<sub>2</sub> on the CH<sub>4</sub> decomposition on the Cu surface and carbon diffusion in the Cu bulk, it is also plausible in Figure 4a,b that the H<sub>2</sub> in the

growth stage could promote the CH<sub>4</sub> decomposition when the H<sub>2</sub> was predissolved into the Cu metal during the heating and annealing steps. We can also find in Figure 4c,d that the single layer graphene was grown without H<sub>2</sub> in the process; however, the Raman D band was somewhat strong with 3 sccm CH<sub>4</sub> indicating the existence of defects; in contrast, increasing the CH<sub>4</sub> flow rate from 3 to 10 sccm suppressed the Raman D band significantly. Thus, our results present a feasible way for the H<sub>2</sub>-free and high-quality graphene growth by using the polycrystalline Cu film and larger CH<sub>4</sub> concentration.

For the Co film, obvious differences can be found. First, it is concluded from Figure 4f–h that the H<sub>2</sub> introduction in the growth step gave thicker and discontinuous graphene flakes, as indicated by SEM images in Figure 2c,d. Then, one can see from Figure 4h,j that only introducing H<sub>2</sub> in the growth step formed the continuous graphene film; additionally, the H<sub>2</sub> participation in the CH<sub>4</sub> decomposition did not increase the graphene thickness, denoting that the H<sub>2</sub> participation in the CH<sub>4</sub> decomposition was contributable to the migration of C atoms on the Co film surface during the nucleation and successive growth of graphene. Hence, all these results suggest that the predissolution of H<sub>2</sub> can enhance the dissolution-in of C atoms (Figure 4f,g), but suppress the diffusion-out (Figure 4g,h).

To get more comprehensive insights into the interaction between carbon and metal atoms with and without H<sub>2</sub>, we first established the calculation models to monitor the energy profiles of carbon monomer diffusing from the metal surface to metal subsurface, as shown in Figure 5, Figure S-3, and Table S-1. In the energy profiles, the benchmark energies  $E_{\text{ref}}$  are based on the models with the lowest energies. It is noted that the models with the C atom adsorbed on the 4-fold hollow sites in

both Cu(100) and Co(100) surfaces are the most stable, which is completely different from the case in the Cu(111) surface.<sup>14,28</sup> As seen in Figure 5a, the configuration with the C atom adsorbed on the Cu(100) surface was more stable by 1.51 eV than that dissolved in the Cu(100) subsurface. Similarly, the state with the C atom adsorbed on the Co(100) surface had a lower energy by 1.87 eV than that in the Co(100) subsurface, as shown in Figure 5b. With the same PBE method, we established the  $2 \times 2$  model for the Cu(111); the enthalpy discrepancy between the models with the carbon adsorbed on the surface fcc sites and subsurface octahedral sites is 0.57 eV. Our PBE result was much bigger than the van der Waals result of 0.37 eV and lower than the LDA result of 0.75 eV,<sup>13</sup> but similar to a value of 0.53 eV reported by other PBE calculations,<sup>28</sup> indicating that our calculation methods are appreciable. Such a big energy difference between (100) and (111) metal (M) surfaces should be primarily ascribed to the crystallography-related coordinated state. That is, in the M(111) surface, the most stable surface adsorbed sites are fcc or hcp, and all the adsorbed sites are three-coordinated with a dangling bond and thus are not stable;<sup>29</sup> but in M(100) surfaces, the surface adsorbed carbon atoms are all tetracoordinated, which will make the surface-adsorbed carbon atom stable. In the light of enthalpy, the carbon dissolutions in M(100) and M(111) are quite different; e.g., the surface formation energy of the Cu(111) surface is 0.13 eV/atom more stable than that of Cu(100).<sup>29</sup> Therefore, the M(100) surface is usually less stable but active as compared to the M(111) surface.<sup>29</sup> It should be added that, prior to the graphene formation on Ni(111)<sup>30</sup> and Cu(111),<sup>28</sup> the incorporation of carbon atom into subsurface interstitial sites is preferable relative to sub-subsurface sites or those deeper ones within the catalyst bulk. Thereby, we only considered the diffusion of carbon atom from the surface to the subsurface of the metals.

For investigating the transition states (TS) during the C atom dissolution, the benchmark formation energy of carbon adsorbed in the Co(100) surface was first calculated as 2.7 eV bigger than that in the Cu(100), denoting a stronger interaction between the carbon and Co surfaces. When the C atoms were dissolved into the metal bulks, the TS states with the C atoms in tetrahedral sites were not stable in both the Cu(100) and the Co(100) surfaces. Specifically, in the Co(100), the C atom at the tetrahedral sites would fall into the bulk octahedral sites spontaneously while relaxing, whereas, after the carbon atoms were adsorbed at the tetrahedral sites in the Cu(100), the surface Cu atoms would reorient changing the tetrahedral sites to a new type of octahedral sites. More details of the new octahedral sites in Cu(100) are discussed in the Supporting Information. By comparison, the calculated energy barriers for the dissolution of C atoms into the Co bulk were much bigger than those in the Cu metal. This data is not in accordance with the bigger C solubility in the Co metal than in the Cu metal. The reason may be that the dissolution of C atoms into the Co metal can lead to the phase transition as reported,<sup>31</sup> which has not been considered within our calculations. After the H<sub>2</sub> predissolution in the subsurface, it is seen that all the TS energies were increased for the Cu(100), but decreased for the Co(100). As a consequence, the H<sub>2</sub> predissolution could enhance the C dissolution into the Co bulk, but conversely in the Cu metal.

To investigate the effects of preadsorbed hydrogen atom concentrations on the interaction between the C and metal atoms, we analyzed four models with hydrogen atomic

concentrations of 0, 25, 75, and 100% in both the Cu(100) and Co(100) surfaces. After they were fully relaxed, we found that if the percentage of predissolved carbon atoms is more than 25% in the Cu(100), the carbon atoms will move together to form C–C bonds and migrate to the surface, leading to structure deformation, as seen in Figure S-4 and Table S-2. In the Co(100) surface, all the structures are stable. Therefore, while comparing the interactions in different metal surfaces, only the models with carbon diffusions of 0 and 25 atom % are listed. Considering that both the ionic interaction and covalence interaction are possibly important during the migration process of carbon atoms, we first performed the charge transfer analysis with the Bader methods. After analysis, the electron numbers occupied on the carbon atom are 4.77 and 4.79 electrons without and with hydrogen atoms adsorbed in the Cu(100), respectively. The corresponding results for the Co(100) were 4.74 and 4.60 electrons without and with the predissolved hydrogen atoms, and the charge amounts of hydrogen atoms were -0.15 in the Cu(100) and -0.20 in the Co(100) after the H<sub>2</sub> predissolution. Therefore, the electrons will slightly transfer from metal to carbon and hydrogen atoms during the carbon and hydrogen migrations in the metal. Also, the hydrogen absorption will dramatically decrease the electrons occupying the carbon atom in the Co(100), which was not found in the Cu(100). Additionally, the electrons occupied on hydrogen atoms were 0.05 bigger in the Co(100) surface than in the Cu(100), showing a strong interaction between hydrogen and Co atoms.

To specify the covalence interactions, we plotted the projected density of states (PDOS) and performed the integrated crystal orbital Hamilton population (iCOHP) analysis, as shown in Figure 6 and Figure 7. In Figure 6, the d band for the Cu metal is lower than the Fermi energy, and the d band for the Co metal crosses the Fermi energy. The main reason is that the d orbital of Co is half-filled with electrons, and that of Cu is fully filled with electrons. After the H<sub>2</sub> predissolution, the d band of Cu metal moves a little, and the

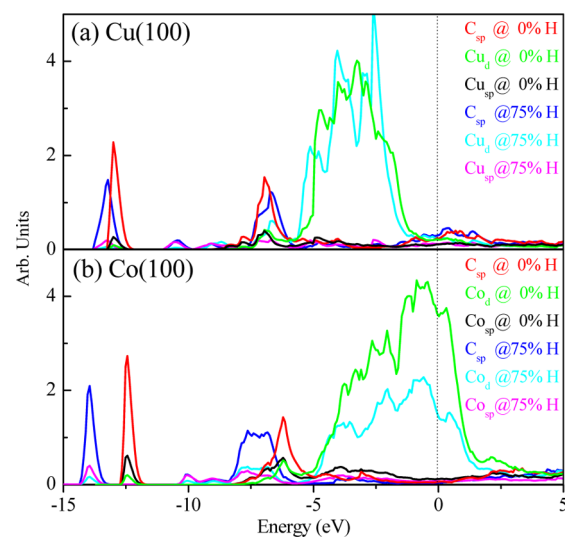


**Figure 6.** Projected density of states (PDOS) of the carbon dissolved metal surface with or without hydrogen predissolution. The 0% percent of hydrogen adsorbed is signed with 0% H, and the model with one carbon and three hydrogen atoms is signed with 75% H. C<sub>sp</sub> represents the total DOS of carbon atoms. The PDOS of metals (Cu and Co) are separated with Cu<sub>d</sub> (Co<sub>d</sub>) and Cu<sub>sp</sub> (Co<sub>sp</sub>).

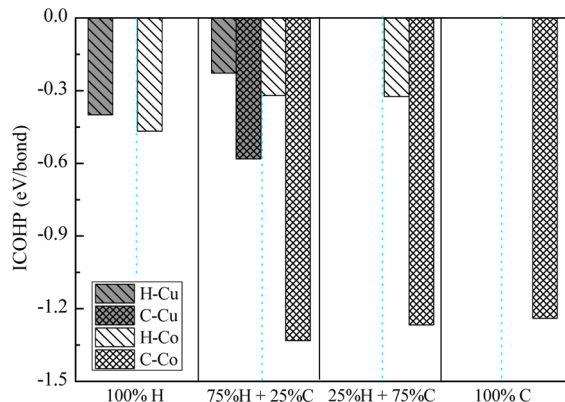


**Figure 7.** Integrated COHP results of Co(100) and Cu(100) surfaces interstitially dissolved with different ratios of C/H atoms.

band of C atom shifts to the lower energy; meanwhile, the main peak of the d band for Co metal is extended and the peak of C atoms is lowered by about 2.0 eV, much larger than that in Cu metal. The iCOHP results are shown in Figure 7. In the absence of H<sub>2</sub>, the iCOHP values of Cu–C and Co–C were calculated as −0.56 and −1.30 eV/bond, respectively, reflecting a much stronger covalence interaction of Co–C atoms. With the increase of H<sub>2</sub> concentration from 25 to 75%, the H–Co covalence interaction was a little changed, but the C–Co covalence interaction was slightly increased. This evidence proves that the H<sub>2</sub> predissolution could improve the C–Co covalence interaction. From the charge analysis and iCOHP results, as a net result, the H<sub>2</sub> predissolution in the Co(100) can enhance the covalence interaction but decrease the ionic interaction between the carbon and metals, but in Cu(100), the effects of hydrogen predissolution on both the ionic interaction and covalence interaction are not obvious.

Summarizing the above experimental and computational results, we can draw a qualitative picture on the role of H<sub>2</sub> on the carbon diffusion in Cu and Co metals. In the Cu film, the predissolved hydrogen atoms, exhibiting weak ionic and covalent interactions with the Cu atoms, affected the interaction negligibly between the carbon and Cu atoms. Also, the H<sub>2</sub> predissolution increased the TS energies in the diffusion of carbon atom. Therefore, it is evidenced that the H<sub>2</sub> predissolution hindered the dissolution of carbon atoms. As a comparison, after the H<sub>2</sub> predissolution, the Co atoms would transfer the electrons to hydrogen atoms thus exhibiting a stronger ionic interaction between the Co and hydrogen atoms and reducing the ionic interaction between the Co and carbon atoms; besides, the H<sub>2</sub> predissolution significantly increased the covalent interaction between the Co and C atoms. Such an increased covalent interaction together with the favorable TS energies should be responsible for the enhanced dissolution of carbon atoms in the experimental data.

## CONCLUSIONS

In conclusion, the roles of H<sub>2</sub> in the carbon dissolution and diffusion-out over Cu and Co films with distinctive carbon solubilities for graphene CVD growth were investigated with experimental and computational results. We specified the effects of H<sub>2</sub> on the crystallographic structure, surface morphology, and chemical environment that are likely to dominate the graphene CVD growth. The interaction between carbon and metal atoms with and without H<sub>2</sub> was monitored with the computational models from the viewpoints of the TS

energies, the projected density of states, the charge transfer, and the integrated COHP. Based on these results, we demonstrate logically that the H<sub>2</sub> predissolution could suppress the carbon dissolution in the Cu film and enhance the diffusion-out of dissolved carbon atoms; conversely, the H<sub>2</sub> predissolution could enhance the carbon dissolution in the Co film and suppress the diffusion-out of dissolved carbon atoms. Our results provide evidence not addressed so far to elucidate the roles of H<sub>2</sub> in the two essential steps of carbon dissolution and diffusion-out in the graphene CVD growth.

## ASSOCIATED CONTENT

### Supporting Information

The Supporting Information is available free of charge on the ACS Publications website at DOI: [10.1021/acs.jpcc.5b07127](https://doi.org/10.1021/acs.jpcc.5b07127).

Statistical grain size and XRD patterns of metal films; computational results and details of metal model deformation, COHP, and PDOS ([PDF](#))

## AUTHOR INFORMATION

### Corresponding Authors

\*E-mail: [hubaoshan@cqu.edu.cn](mailto:hubaoshan@cqu.edu.cn) (B.H.).

\*E-mail: [bshang@cqu.edu.cn](mailto:bshang@cqu.edu.cn) (B.S.).

### Notes

The authors declare no competing financial interest.

## ACKNOWLEDGMENTS

This work was financially supported by the National Natural Science Foundation of China (Nos. 51502026, 51272296, and 41201546), the Natural Science Foundation of Chongqing (No. CSTC2012jjA50014, CSTC2012jjA20010), the Scientific Research Foundation for the Returned Overseas Chinese Scholars (No. 2013-693), the Specialized Research Fund for the Doctoral Program of Higher Education of China (No. 20130191120043), and the Fundamental Research Funds for the Central Universities (Nos. CQDXWL-2013016 and CQDXWL-2014001). The authors are also grateful to the Research Grant Council of Hong Kong SAR (Nos. 623512 and DAG12EG05) for financial support.

## REFERENCES

- (1) Yan, K.; Fu, L.; Peng, H.; Liu, Z. Designed CVD Growth of Graphene via Process Engineering. *Acc. Chem. Res.* **2013**, *46*, 2263–2274.
- (2) Wu, B.; Geng, D.; Xu, Z.; Guo, Y.; Huang, L.; Xue, Y.; Chen, J.; Yu, G.; Liu, Y. Self-Organized Graphene Crystal Patterns. *NPG Asia Mater.* **2013**, *5*, e36.
- (3) Zhang, Y.; Li, Z.; Kim, P.; Zhang, L.; Zhou, C. Anisotropic Hydrogen Etching of Chemical Vapor Deposited Graphene. *ACS Nano* **2012**, *6*, 126–132.
- (4) Geng, D.; Wu, B.; Guo, Y.; Luo, B.; Xue, Y.; Chen, J.; Yu, G.; Liu, Y. Fractal Etching of Graphene. *J. Am. Chem. Soc.* **2013**, *135*, 6431–6434.
- (5) Vlassiuk, I.; Regmi, M.; Fulvio, P.; Dai, S.; Datskos, P.; Eres, G.; Smirnov, S. Role of Hydrogen in Chemical Vapor Deposition Growth of Large Single-Crystal Graphene. *ACS Nano* **2011**, *5*, 6069–6076.
- (6) Zhang, X.; Ning, J.; Li, X.; Wang, B.; Hao, L.; Liang, M.; Jin, M.; Zhi, L. Hydrogen-Induced Effects on the CVD Growth of High-Quality Graphene Structures. *Nanoscale* **2013**, *5*, 8363–8366.
- (7) Ma, T.; Ren, W.; Zhang, X.; Liu, Z.; Gao, Y.; Yin, L. C.; Ma, X. L.; Ding, F.; Cheng, H. M. Edge-Controlled Growth and Kinetics of Single-Crystal Graphene Domains by Chemical Vapor Deposition. *Proc. Natl. Acad. Sci. U. S. A.* **2013**, *110*, 20386–20391.

- (8) Mohsin, A.; Liu, L.; Liu, P.; Deng, W.; Ivanov, I. N.; Li, G.; Dyck, O. E.; Duscher, G.; Dunlap, J. R.; Xiao, K.; Gu, G. Synthesis of Millimeter-Size Hexagon-Shaped Graphene Single Crystals on Resolidified Copper. *ACS Nano* **2013**, *7*, 8924–8931.
- (9) Gan, L.; Luo, Z. Turning off Hydrogen to Realize Seeded Growth of Subcentimeter Single-Crystal Graphene Grains on Copper. *ACS Nano* **2013**, *7*, 9480–9488.
- (10) Yan, Z.; Liu, Y.; Lin, J.; Peng, Z.; Wang, G.; Pembroke, E.; Zhou, H.; Xiang, C.; Raji, A. R. O.; Samuel, E. L.; et al. Hexagonal Graphene Onion Rings. *J. Am. Chem. Soc.* **2013**, *135*, 10755–10762.
- (11) Jin, Y.; Hu, B. S.; Wei, Z.; Luo, Z.; Wei, D.; Xi, Y.; Zhang, Y.; Liu, Y. Roles of H<sub>2</sub> in Annealing and Growth Times of Graphene CVD Synthesis over Copper Foil. *J. Mater. Chem. A* **2014**, *2*, 16208–16216.
- (12) Losurdo, M.; Giangregorio, M. M.; Capezzuto, P.; Bruno, G. Graphene CVD Growth on Copper and Nickel: Role of Hydrogen in Kinetics and Structure. *Phys. Chem. Chem. Phys.* **2011**, *13*, 20836–20843.
- (13) Zhang, X.; Wang, L.; Xin, J.; Yakobson, B. I.; Ding, F. Role of Hydrogen in Graphene Chemical Vapor Deposition Growth on a Copper Surface. *J. Am. Chem. Soc.* **2014**, *136*, 3040–3047.
- (14) Li, K.; He, C.; Jiao, M.; Wang, Y.; Wu, Z. A First-Principles Study on the Role of Hydrogen in Early Stage of Graphene Growth During the CH<sub>4</sub> Dissociation on Cu(111) and Ni(111) Surfaces. *Carbon* **2014**, *74*, 255–265.
- (15) Tian, J.; Hu, B.; Wei, Z.; Jin, Y.; Xia, M.; Pan, Q.; Liu, Y.; Luo, Z. Surface Structure Deduced Differences of Copper Foil and Film for Graphene CVD Growth. *Appl. Surf. Sci.* **2014**, *300*, 73–79.
- (16) Lin, H. C.; Chen, Y. Z.; Wang, Y. C.; Chueh, Y. L. The Essential Role of Cu Vapor for the Self-Limit Graphene via the Cu Catalytic CVD Method. *J. Phys. Chem. C* **2015**, *119*, 6835–6842.
- (17) Koinuma, M.; Ogata, C.; Kamei, Y.; Hatakeyama, K.; Tateishi, H.; Watanabe, Y.; Taniguchi, T.; Gezuhara, K.; Hayami, S.; Funatsu, A.; et al. Photochemical Engineering of Graphene Oxide Nanosheets. *J. Phys. Chem. C* **2012**, *116*, 19822–19827.
- (18) Leconte, N.; Moser, J.; Ordejon, P.; Tao, H.; Lherbier, A.; Bachtold, A.; Alsina, F.; Sotomayor Torres, C. M.; Charlier, J. C.; Roche, S. Damaging Graphene with Ozone Treatment: A Chemically Tunable Metal–Insulator Transition. *ACS Nano* **2010**, *4*, 4033–4038.
- (19) Samarakoon, D. K.; Wang, X. Q. Twist-Boat Conformation in Graphene Oxides. *Nanoscale* **2011**, *3*, 192–195.
- (20) Nourbakhsh, A.; Cantoro, M.; Vosch, T.; Pourtois, G.; Clemente, F.; van der Veen, M. H.; Hofkens, J.; Heyns, M. M.; De Gendt, S.; Sels, B. F. Bandgap Opening in Oxygen Plasma-Treated Graphene. *Nanotechnology* **2010**, *21*, 435203–435211.
- (21) Vinogradov, N.; Schulte, K.; Ng, M. L.; Mikkelsen, A.; Lundgren, E.; Mårtensson, N.; Preobrajenski, A. Impact of Atomic Oxygen on the Structure of Graphene Formed on Ir(111) and Pt(111). *J. Phys. Chem. C* **2011**, *115*, 9568–9577.
- (22) Acik, M.; Lee, G.; Mattevi, C.; Pirkle, A.; Wallace, R. M.; Chhowalla, M.; Cho, K.; Chabal, Y. The Role of Oxygen during Thermal Reduction of Graphene Oxide Studied by Infrared Absorption Spectroscopy. *J. Phys. Chem. C* **2011**, *115*, 19761–19781.
- (23) Aria, A. I.; Gani, A. W.; Gharib, M. Effect of Dry Oxidation on the Energy Gap and Chemical Composition of CVD Graphene on Nickel. *Appl. Surf. Sci.* **2014**, *293*, 1–11.
- (24) Shin, Y. C.; Kong, J. Hydrogen-Excluded Graphene Synthesis via Atmospheric Pressure Chemical Vapor Deposition. *Carbon* **2013**, *59*, 439–447.
- (25) Ryu, J.; Kim, Y.; Won, D.; Kim, N.; Park, J. S.; Lee, E. K.; Cho, D.; Cho, S. P.; Kim, S. J.; Ryu, G. H.; et al. Fast Synthesis of High-Performance Graphene Films by Hydrogen-Free Rapid Thermal Chemical Vapor Deposition. *ACS Nano* **2014**, *8*, 950–956.
- (26) Peng, K. J.; Wu, C. L.; Lin, Y. H.; Liu, Y. J.; Tsai, D. P.; Pai, Y. H.; Lin, G. R. Hydrogen-Free PECVD Growth of Few-Layer Graphene on an Ultra-Thin Nickel Film at the Threshold Dissolution Temperature. *J. Mater. Chem. C* **2013**, *1*, 3862–3870.
- (27) Jung, D. H.; Kang, C.; Kim, M.; Cheong, H.; Lee, H.; Lee, J. S. Effects of Hydrogen Partial Pressure in the Annealing Process on Graphene Growth. *J. Phys. Chem. C* **2014**, *118*, 3574–3580.
- (28) Riikonen, S.; Krasheninnikov, A.; Halonen, L.; Nieminen, R. The Role of Stable and Mobile Carbon Adspecies in Copper-Promoted Graphene Growth. *J. Phys. Chem. C* **2012**, *116*, 5802–5809.
- (29) Da Silva, J. L.; Barreteau, C.; Schroeder, K.; Blügel, S. All-Electron First-Principles Investigations of the Energetics of Vicinal Cu Surfaces. *Phys. Rev. B: Condens. Matter Mater. Phys.* **2006**, *73*, 125402.
- (30) Weatherup, R. S.; Amara, H.; Blume, R.; Dlubak, B.; Bayer, B. C.; Diarra, M.; Bahri, M.; Cabrero-Vilatela, A.; Caneva, S.; Kidambi, P. R.; et al. Interdependency of Subsurface Carbon Distribution and Graphene–Catalyst Interaction. *J. Am. Chem. Soc.* **2014**, *136*, 13698–13708.
- (31) Ciobică, I.; van Santen, R. A.; van Berge, P.; van de Loosdrecht, J. Adsorbate Induced Reconstruction of Cobalt Surfaces. *Surf. Sci.* **2008**, *602*, 17–27.